Journal of Sound and Vibration 332 (2013) 1172–1187

Contents lists available at SciVerse ScienceDirect

Journal of Sound and Vibration

journal homepage: www.elsevier.com/locate/jsvi

Acoustic topology optimization of fibrous material with Delany–Bazley empirical material formulation

Gil Ho Yoon

School of Mechanical Engineering, Hanyang University, Seoul, Republic of Korea

ARTICLE INFO

Article history:
Received 15 September 2011
Received in revised form
10 October 2012
Accepted 15 October 2012
Handling Editor: L. Huang
Available online 17 November 2012

ABSTRACT

This research details a new acoustic topology optimization (ATO) framework with an empirical material formulation for fibrous material. Despite the importance of considering pressure attenuation not only by internal solid structures but also by fibrous (porous) structures in acoustic design, a systematic ATO approach with an empirical material formulation has not yet been proposed. Thus, in this paper, an empirical material formulation called the Delany–Bazley model is implemented for the development of an ATO framework for fibrous material with porosity close to 1. By means of the SIMP (solid isotropic material with penalization) interpolation functions developed for multiple structural materials, ATO processes for fibrous structures as well as internal solid structures are carried out. In addition, a heuristic filter method that allows fibrous material to emerge only at the boundaries or rims of an internal solid structure is presented. Finally, the effect of the pressure attenuation on the topological layout for fibrous materials is investigated by solving several illustrative topology optimization examples.

1. Introduction

This research presents a new acoustic topology optimization (ATO) framework that solves the Helmholtz equation with a representative empirical material formulation, called the Delany–Bazley model, for fibrous material with porosity close to 1. To improve the static and dynamic characteristics of various engineering structures systematically, size, shape and topology optimization (TO) methods have been introduced and a number of papers have been published on their various engineering applications including ATO [1–9]. Despite some researches relevant to the TO of acoustic and acoustic–structure systems, ATO with an empirical acoustic formulation for fibrous materials has not yet been researched. Indeed, this research focuses on the introduction and application of the empirical material formulation to ATO for the first time.

This research adopts an empirical material formulation of fibrous material for ATO. In industry and daily life, excessive noise can lead to adverse health problems such as hearing loss, sleep disturbances, and psychological issues, making it a non-negligible source of environmental pollution. Consequently, public health issues caused by loud and irritating noises are now being treated seriously, and many engineering approaches are being explored to help resolve the environmental pollution concerns. For example, one common engineering approach is to properly shield and protect noise sources by using acoustic or fibrous materials [10–12]. Fibrous materials are very effective at reducing the noise level or controlling the noise direction and hence, have been widely utilized in music studios and automotive shops. They are now being further engineered to resolve broader noise issues. Commonly, these engineered acoustic materials consist of fibrous textures or plastic forms (having a porosity close to 1 and an almost rigid form), which are effective at pressure attenuation. From a mathematical point of view, the pressure attenuation by these acoustic materials can be characterized by a complex acoustic impedance and a complex density in an acoustic simulation of the Helmholtz equation. However,

E-mail addresses: ghy@hanyang.ac.kr, gilho.yoon@gmail.com

0022-460X/$ - see front matter © 2012 Elsevier Ltd. All rights reserved.
http://dx.doi.org/10.1016/j.jsv.2012.10.018

these complex acoustic impedances and densities show different behaviors with respect to the wide range of excitation frequencies that are typical of fibrous materials, making analytical formulations nearly impossible to derive. In general, methods that consider fluid and structure interaction on both micro and macro scales, such as the homogenization method, are inadequate [13]. To our best knowledge, currently available acoustic models used for acoustic simulation can be roughly divided into three kinds: the empirical material model, the phenomenological material model, and the microstructure material model; see Refs. [13,14] for more details. Among these three acoustic material models, the empirical material models require fewer acoustic parameters of porous materials, and are widely accepted for the application of very highly porous materials for specific frequency ranges. Several empirical material models, such as the Delany–Bazley model, Miki model [15], and Allard and Champoux model [16], have been developed from extensive experimental investigations. Sometimes the physical structure of the fibrous material to be measured is known a priori and this geometric information can be used to increase the accuracy and reliability of the empirical material models [13]. Note that although empirical material models are simple to use in numerical and practical application solutions, they do not generally give reliable predicted results over the entire utilized frequency range, rendering them less practical. Nevertheless, because the empirical material models are efficient from an analysis and optimization point of view, ATO is performed using these empirical material formulations with complex bulk modulus and densities in this research.

Sound and pressure absorption by fibrous materials strongly depends on the materials' position and placement. In other words, higher pressure attenuation can be achieved by placing absorptive fibrous materials at optimal and proper locations. For example, in a rectangular room, fibrous absorbers placed near the corners and along the twelve room edges are known to be very effective in reducing the noise level [17]. Similarly, in a speech or music studio or a lecture room, it is better to cover the areas at eye-level on the side walls with fibrous patches or textures to achieve higher pressure attenuation, as shown in Fig. 1. For an example, Fig. 1(c) shows fibrous panels installed in a lecture room in Hanyang University to minimize reflected sound from wall. Indeed, the optimal placement of these fibrous materials is an important engineering issue, but it generally appears to be achieved via a trial-and-error approach; a systematic ATO approach with the empirical material models has yet to be developed. Instead of producing costly combinations of porous media and choosing the best acoustic design after they have been implemented, a systematic ATO approach would yields suggestions for a few very good candidates before time and materials have been wasted.

A few relevant studies have been done to improve the acoustic performances in engineering structures [4,18–23]. In these studies, fibrous materials are typically characterized by their porosity, frame flexibility, tortuosity, which accounts for curved pore-lengths, and other pore-shape factors, particularly those that consider pore shapes other than cylinders. Depending on the influences of these characteristics, many experimental and analytical formulations have already been developed and structural

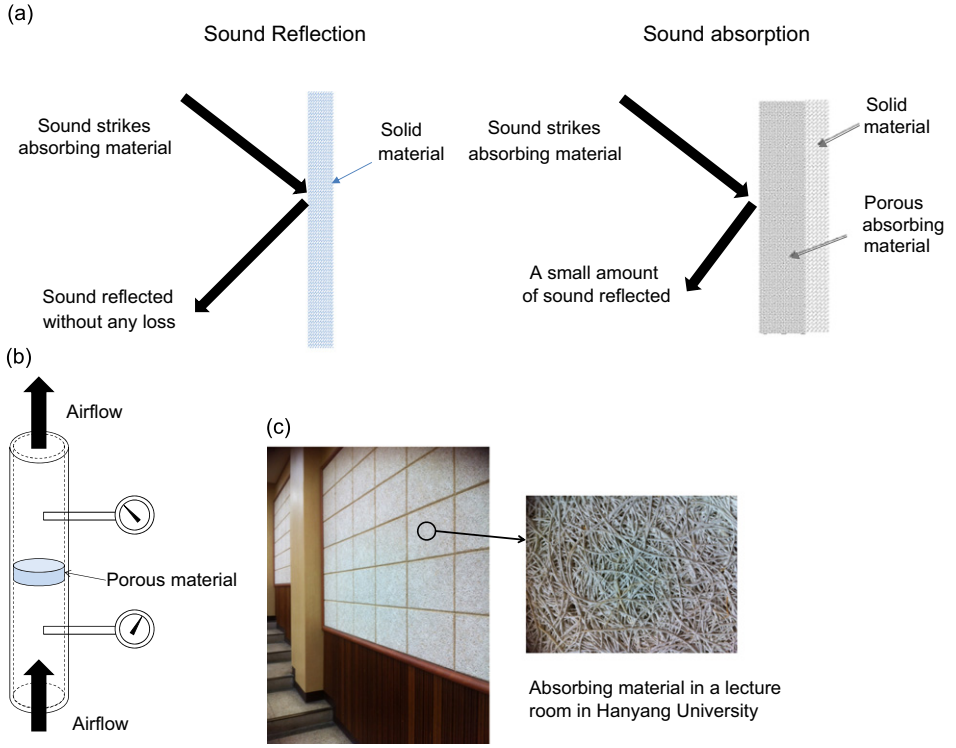

Fig. 1. Examples and applications of absorptive porous materials. (a) A comparison of the reflected sounds by a solid (rigid) wall versus an absorptive wall, (b) a drawing of the impedance tube method, used to measure the airflow resistivity of the porous materials and (c) an application of fibrous material in a lecture room in Hanyang University.

optimization schemes based on these formulations have been proposed. For instance, Yoon et al. presented a TO framework using a mixed finite-element formulation that considered the acoustic–structure interaction on a macro scale [4]. Dühring et al. [24] and Lee and Kim [23], on the other hand, presented TO approaches to design the internal rigid structure inside an acoustic domain by interpolating the density and bulk modulus of the Helmholtz equation in order to minimize the sound pressure of a specified area without considering the fluid–structure interaction. By parameterizing the complex boundary conditions with respect to the additional TO design variables, the approach of Dühring et al. [24] allows for the design of optimal absorptive boundary conditions. Alternatively, Kim et al. [19,20] proposed a TO scheme that considered the fluid–structure interaction between a porous elastic frame and air, which is governed by the simplified FSI equation known as Biot's theory [13,25]. Then, Yamamoto et al. performed ATO with multiple materials, based on Biot's theory, in order to minimize the sound pressure level [21]. Du and Olhoff [26] utilized a simplified acoustic pressure radiation model of plates for TO. Finally, Akl et al. applied acoustic topology optimization for a plate coupled with an acoustic cavity and verified their designs with experiments [27]. The research presented below adds to these works by examining fibrous material models and optimizing layouts of both fibrous and solid structures from a materials-distribution perspective in the acoustic domain.

To our best knowledge, there is no ATO research that utilizes an empirical material model, such as the Delany–Bazley model, that is efficient in calculating the pressure attenuation for engineered fibrous material. Compared with the accuracy and numerical difficulties of Biot's theory, which considers the fluid–structure interaction between air and the elastic frame of fibrous material on a microscopic scale, the empirical material models are quite accurate for porosities close to one [13]. Moreover, the Helmholtz equation requires only the numerical solution for these empirical material models, whereas Biot's theory and other acoustic simulation theories involve relatively complex fluid and structure equations, several material variables, and inevitably, numerous degrees of freedom. Consequently, it is expected that computational efficiency can be obtained with the empirical fibrous model in ATO.

The layout of the paper is organized as follows: first, we review the acoustic analysis with the empirical material model. Then, we present the ATO formulation as well as the material interpolation schemes for ATO in Section 3. In the numerical analysis section, we provide a few topology optimization examples that demonstrate the validity and potential of the developed ATO. Finally, we summarize and discuss our findings in the conclusion.

2. Finite element analysis for an acoustic system using an empirical material formulation

For an ideal, incompressible (low Mach number) fluid flow that neglects sound absorption and sound attenuation due to fluid viscosity, the governing equation of the harmonically varying pressure (i.e., $\tilde{p}(t)=p\,e^{i\omega t}$) in an inhomogeneous acoustic medium, Ω_a, can be written as follows:

$$\nabla\cdot\left(\frac{1}{\rho}\nabla p\right)+\frac{\omega^2 p}{\rho c^2}=0,\quad \left(k=\frac{\omega}{c}\right)\quad \text{on } \Omega_a \tag{1}$$

where p, ρ, and c are the spatially-varying pressure in the acoustic domain Ω_a, the density of the acoustic domain, and the local speed of sound, respectively. The spatial differential operator is ∇. The angular velocity and the wavenumber are denoted by ω and k, respectively. The pressure field can then be computed by solving the above Helmholtz equation with the following proper boundary conditions:

$$\textit{Pressure boundary condition}: \quad p=p_0 \tag{2}$$

$$\textit{Hard wall condition}: \quad \mathbf{n}\cdot\nabla p=0 \tag{3}$$

$$\textit{Acceleration boundary condition}: \quad \mathbf{n}\cdot\nabla p=a_n \tag{4}$$

$$\textit{Sommerfeld boundary condition}: \quad \mathbf{n}\cdot\nabla p+i\cdot k\cdot p=2i\cdot k\cdot p_{\text{in}} \tag{5}$$

where p_0, $\mathbf{n}$, a_n, and p_{in} are the pressure input, the outward unit normal to the acoustic domain, the input acceleration, and the pressure amplitude of the incoming wave, respectively. To simulate the wave propagation boundary condition without reflection (i.e., having anechoic termination after an acoustic propagation), the Sommerfeld boundary condition in Eq. (5) can be applied using $p_{\text{in}}=0$; see Ref. [10] for an actual finite element implementation code.

Before proceeding further, we must introduce the concept of the specific acoustic impedance, which represents the basic characteristics of the acoustic domain of interest. The specific acoustic impedance, Z, is defined as the ratio of the acoustic pressure (p) to the associated fluid speed (u) as follows:

$$Z=p/u=R_z+X_z i \tag{6}$$

where R_z and X_z are the specific acoustic resistance and the specific acoustic reactance of the acoustic domain, respectively. By confining our consideration to the ideal non-dissipated wave propagation, Z becomes ρc.

Applying the minimum potential theory to the Helmholtz equation, the following finite-element stiffness and mass matrices can be obtained:

$$\mathbf{k}_e=\int\frac{1}{\rho_e}\nabla\mathbf{N}^{\mathrm{T}}\nabla\mathbf{N}\,d\Omega,\quad \mathbf{m}_e=\int\frac{1}{k_e^{\text{bulk}}}\mathbf{N}^{\mathrm{T}}\mathbf{N}\,d\Omega\quad (k_e^{\text{bulk}}=\rho_e c^2) \tag{7}$$

$$\mathbf{K} = \underset{e=1}{\overset{NE}{\mathbf{A}}} \mathbf{k}_e, \quad \mathbf{M} = \underset{e=1}{\overset{NE}{\mathbf{A}}} \mathbf{m}_e \tag{8}$$

where the finite-element shape function is denoted by **N** and the matrix assembly operator is denoted by **A** for *NE* finite elements. The stiffness and mass matrices for the *e*th element are denoted by $\mathbf{k}_e$ and $\mathbf{m}_e$, respectively. The element constant density and the bulk modulus of the *e*th element are denoted by ρ_e and k_e^{bulk}, respectively. After formulating the finite-element matrices using the appropriate boundary conditions for fibrous materials, the following matrix form can be written without loss of generality:

$$[\mathbf{K}(\omega) - \omega^2 \mathbf{M}(\omega)]\mathbf{X} = \mathbf{F}(\omega) \tag{9}$$

In the context of the finite-element procedure, the pressure vector and the force vector are denoted by **X** and **F**, respectively. The frequency-dependent stiffness and mass matrices are denoted by **K** and **M**, respectively.

2.1. Porous material: Delany–Bazley material model for fibrous materials with porosities close to 1[1]

For most acoustic engineering problems, it is a valid assumption that the dissipation of acoustic energy is small enough to neglect its effect on the acoustic wave flow in Eq. (1). However, in some particular computational simulations with porous materials, the energy dissipation from the absorption and attenuation of sound pressure by porous materials cannot be neglected and should be included in the simulation [12,15,28–30]. Unfortunately, the geometries of the pores in ordinary porous materials are too complex and random to perform a direct calculation of the viscous and thermal interactions between the air and these fibrous materials.[2] For these reasons, a simple-to-calculate empirical material formulation is often used for acoustic simulations. Among the many empirical material models, the Delany–Bazley material model is one of the most representative empirical material formulations for porous absorbing materials such as fiber and wood-wool, particularly for considering the effects of sound-absorptive materials with porosities close to one on acoustic pressure attenuation, and can be presented as follows:

$$k_c = k_a\left(1 + 0.0978\left(\frac{\rho_a f}{\sigma}\right)^{-0.7} - \mathrm{i}0.189\left(\frac{\rho_a f}{\sigma}\right)^{-0.595}\right) \tag{10}$$

$$Z_c = Z_a\left(1 + 0.057\left(\frac{\rho_a f}{\sigma}\right)^{-0.734} - \mathrm{i}0.087\left(\frac{\rho_a f}{\sigma}\right)^{-0.732}\right) \tag{11}$$

$$c_c = \frac{\omega}{k_c}, \quad \rho^c = \frac{k_c Z_c}{\omega}, \quad f = \frac{\omega}{2\pi}, \quad 0.01 < \left(\frac{\rho_a f}{\sigma}\right) < 1.0 \tag{12}$$

where the wavenumber and the density of air without pressure attenuation are denoted by k_a and ρ_a, respectively. The complex wavenumber and impedance of the Delany–Bazley empirical material model are k_c and Z_c, respectively. The coefficients of the above equations were obtained and tuned via experiments conducted by Delany and Bazley. Note that the empirical material formulation shown in Eqs. (10)–(12) is based only on measurements of the bulk airflow resistivity, σ, which is highly dependent on the chosen fibrous material in Fig. 1(b) [31,32]. To obtain this airflow resistivity, the experiment in Fig. 1(b) is conducted. For example, the airflow resistivity of soft fireboard is typically in the region of 5 million Rayleighs/m while that of wood-wool is in the region of 1000 Rayleighs/m. Likewise, most practical porous glass fibrous material has been designed with an airflow resistivity in the range of 10^5–10^6 Rayleighs/m. Because of its simplicity in numerical implementation, this empirical material model has long enjoyed a wide acceptance and works well for fibrous materials over a normalized frequency range of $\rho_a f/\sigma$ from 0.01 to 1. It is also known that it works well for wood-wool and porous materials with open-cell forms [13].

Nevertheless, the above relations do not necessarily provide a suitable prediction of the acoustic behavior of all porous materials in all frequency ranges—in particular, for $\rho_a f/\sigma$ greater than 1 or less than 0.01 [29,31]. In other words, the above Delanzy–Bazley model does not consider the stacked directions of fibers and assumes that a fibrous form is geometrically homogeneous in terms of the wavenumber and impedance. Recently, several researchers have noted that the coefficients predicted by Delany and Bazley are not especially accurate when applied to poroelastic materials (i.e., not rigid frame materials), and Miki in [15] and Allard and Champoux in [16] have obtained different coefficients that improve the prediction accuracy of the Delany and Bazley model. To develop a more elaborate form that incorporates the elastic frame and the directionality of the fibers, other quantities such as tortuosity and the shapes of the holes inside the fibrous material should be considered [13,29]. For the application of ATO, only the above Delany–Bazley material model is considered here. Although they were not tested for this study, it is reasonable to assume that similar methods could be easily extended to the other empirical material models. Moreover, from a finite-element (FE) method point of view, the

[1] The porosity is defined as the ratio of the air volume to the total volume of porous material. For most of the fibrous materials and plastic forms with open bubbles, the porosity is very close to one.

[2] With the simplified modeling of sound propagation in pores, the influence of the viscous interaction of the air on the density and the influence of the thermal interaction of the air on the bulk modulus can be derived [13].

formulations by Delany and Bazley are also suitable for incorporating directly into the FE procedure; it is just a matter of substituting the sound speed and the density from Eq. (1) with the complex sound speed and the complex density.

2.2. Numerical example

To test the effects of fibrous materials on pressure attenuation, the elementary muffler example shown in Fig. 2 was considered. At the left inlet and the right outlet, Sommerfeld boundary conditions were imposed. Note that the characteristics of this two-dimensional expansion muffler without fibrous materials, including the analytical transmission loss (TL) curve, are well-studied [10]. Thus, the incoming wave pressure was first calculated using

$$p_i = \frac{1}{e^{ikx_1}} \frac{p_1 - p_2 e^{-ikx_{12}}}{1 - e^{-i2kx_{12}}} \quad (p_1 = p_i e^{ikx_1} + p_r e^{-ikx_1} p_2 = p_i e^{ikx_2} + p_r e^{-ikx_2}) \tag{13}$$

where p_1 and p_2 are the complex pressures at the arbitrary points of the inlet and the distance between the two points ($x=x_1$, $x=x_2$) is x_{12} as shown in Fig. 2. The magnitudes of the incoming and the reflected waves are denoted by p_i and p_r, respectively. Then, the transmission loss of the acoustic muffler was approximated using the ratio of the incoming wave

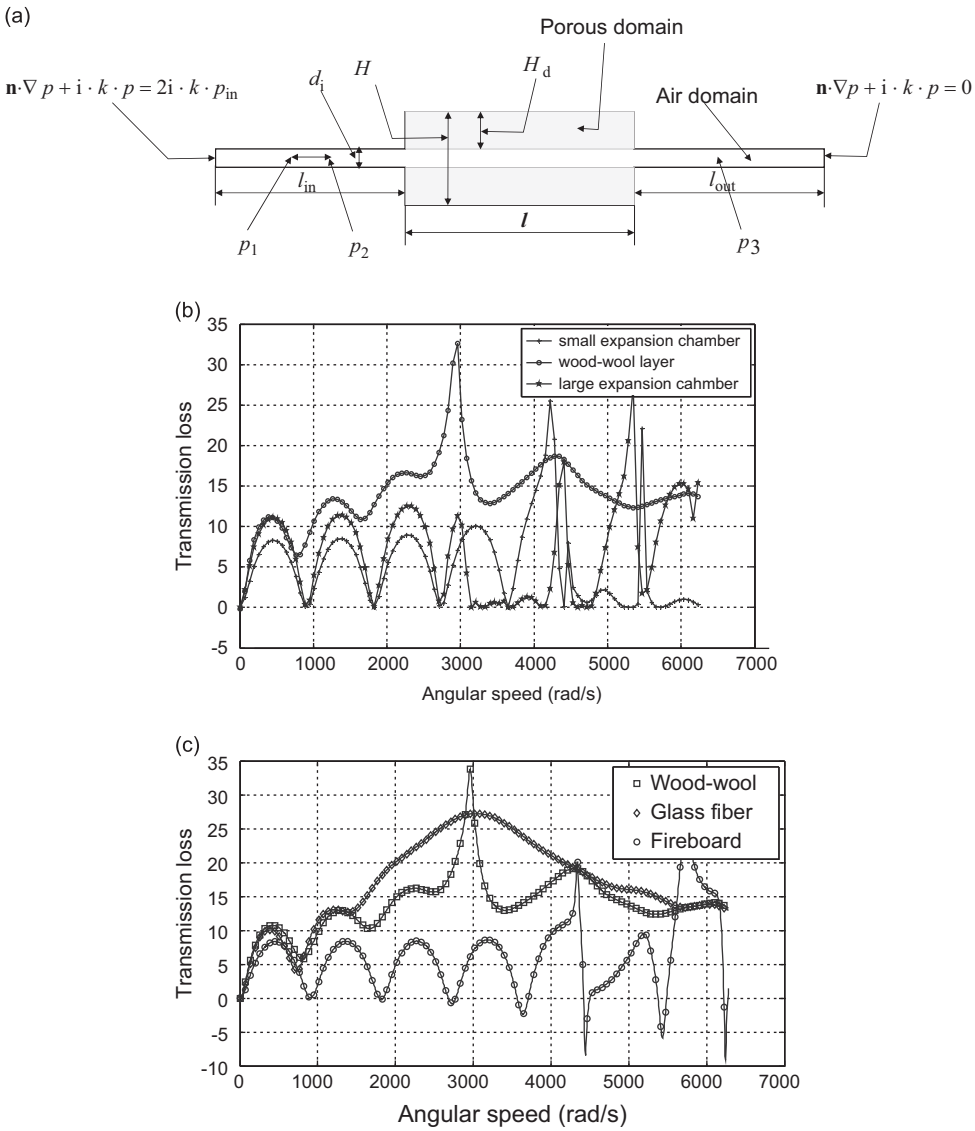

Fig. 2. A 2D muffler analysis example with the Delany–Bazley model. (a) Muffler geometry ($\rho_a=1.25$ kg/m^3, $c_a=343$ m/s, $\sigma=1000$ Rayleighs/m, $l=1.2$ m, $l_{in}=l_{out}=1.0$ m, $H_d=0.2$ m, $H=0.5$ m, $d_i=0.1$ m, $x_{12}=0.1$ m, $\sigma=1000$ Rayleighs/m), (b) the transmission loss curves with and without the fibrous material layer (small expansion chamber: $H_d=0.0$ m, $H=0.5$ m, large expansion chamber: $H_d=0.0$ m, $H=0.7$ m, wood-wool chamber: $H_d=0.1$ m, $H=0.7$ m), and (c) the transmission loss curves for several flow resistivity values ($\sigma_{\text{wood-wool}}=1000$, $\sigma_{\text{Glass}}=10{,}000$, $\sigma_{\text{Fireboard}}=5{,}000{,}000$).

pressure to the transmitted wave pressure such that

$$\mathrm{TL} = 20\log\left(\left|\frac{p_i}{p_3}\right|\right) + 10\log\left(\left|\frac{A_i}{A_o}\right|\right) \tag{14}$$

where the complex pressure output at the outlet is denoted by p_3. The areas of the inlet and outlet tubes are denoted by A_i and A_o, respectively. The above method is called the three-point method. One of the shortcomings of the above method is that there is the large discrepancy for higher frequencies at which the one-dimensional inlet pressure calculation of Eq. (13) is not valid anymore. Fig. 2(b) shows the calculated transmission loss for the mufflers with and without the fibrous material layers ($\sigma = 1000$ Rayleighs/m) at the two sides of the chamber as well as their transmission curves for the given configurations. As shown, by attaching the Delany–Bazley fibrous layers to the top and bottom sides of the expansion chamber, a higher pressure attenuation was achieved compared to that without the fibrous layers. Fig. 2(c) shows the TL curves for various porous materials. It is observed from the calculated data that the peaks of the TL curve at higher frequencies are suppressed when the porous materials are used. The average TL values are increased substantially and as expected the TL performance is improved by increasing the flow resistance [33]. It is also noticed that it is intricate to explain sound wave propagation in porous materials because of the complex characteristics of the porous material such as pore size, frame orientation, pore interconnection elasticity and the pore cross-section represented by the flow resistivity values in the Delany–Bazley model.

3. Acoustic topology optimization formulation

Mathematically, the original ATO is a discrete optimization problem. In other words, each point of an acoustic design domain should be either air, solid or fibrous material that can only be solved by discrete or integer optimization algorithms such as genetic algorithms or simulated annealing [1,22]. In order to use an efficient gradient-based optimizer, the original discrete optimization problem must be reformulated using the relaxed continuous material properties that are interpolated from the bulk material properties of these three states with respect to the TO design variables. In the conventional ATO, the density and the bulk modulus are interpolated with respect to design variables and an optimization algorithm distributes materials to find out acoustic domain and wall domain as shown in Fig. 3(a). In the present approach, using the conventional SIMP-based interpolation functions for multiple materials, the three states – air, solid, and fibrous material – are obtained as shown in Fig. 3(b). Furthermore, new heuristic interpolation functions for fibrous material attached to solid structures are presented in this section.

3.1. Acoustic topology optimization formulation

In this research, the following optimization formulation that minimizes an objective function subject to mass constraints is used for ATO:

$$\text{Min } \phi(\mathbf{X}) \tag{15}$$

$$\begin{aligned} \text{Subject to} \quad & \sum_{e=1}^{NE} \gamma_{e,1} v_e \Big/ \sum_{e=1}^{NE} v_e - \beta_{\text{solid}} \le 0 \\ & \sum_{e=1}^{NE} \gamma_{e,2} v_e \Big/ \sum_{e=1}^{NE} v_e - \beta_{\text{fibrous}} \le 0 \\ & \boldsymbol{\gamma} = \Big[\underbrace{\gamma_{1,1}, \cdots, \gamma_{NE,1}}_{\text{For solid structure}}, \underbrace{\gamma_{1,2}, \cdots, \gamma_{NE,2}}_{\text{For fibrous structure}} \Big] \end{aligned} \tag{16}$$

where $\mathbf{X}$ and $\boldsymbol{\gamma}$ are the acoustic pressure vector calculated by Eq. (9) and the $NE \times 2$ design variables, respectively. The

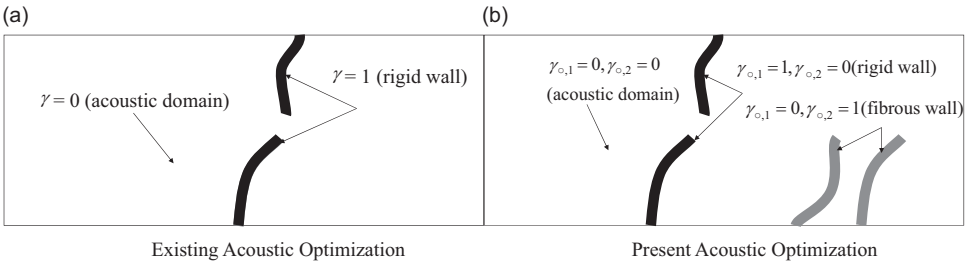

Fig. 3. The concept of acoustic topology optimization: (a) An existing acoustic optimization and (b) the present acoustic optimization.

objective function and the allowable mass ratios of the solid material and the fibrous material are denoted by ϕ, β_{solid}, and β_{fibrous}, respectively. The volume of the eth element is represented by v_e, and two design variables, $\gamma_{e,1}$ and $\gamma_{e,2}$, are assigned for each element. When the first and second design variables are given the values of 1 and 0, respectively, then the corresponding element will be modeled as a solid element. Conversely, when the design variables are 0 and 1, respectively, then the element will be modeled as a fibrous element. When the two design variables are both zeroes, the corresponding element must be modeled as an air element. In the above optimization formulation, the mass constraints to each material are employed to restrict the amount of materials used from an economical point of view. Furthermore, it is common to use the mass constraint(s) in conventional topology optimization framework.

3.2. SIMP-based material interpolation scheme for multiple materials

In order to conduct ATO with the empirical material formulation, the two material properties – i.e., the density and the bulk modulus – of the Helmholtz equation are interpolated with respect to the design variables, as shown in Table 1. To interpolate the three physical states (air, solid and fibrous material) the interpolation functions from Eqs. (17)–(19) can be employed without loss of generality. It is worthwhile to note first that these SIMP-based polynomial interpolation functions for multiple TO materials are used with two design variables for each element. Second, the reciprocal density and the reciprocal bulk modulus are interpolated with respect to the design variables. For this second issue, several numerical tests and interpolation functions have been proposed by Lee and Kim [23]. It seems obvious to employ the reciprocals of these material properties since these values are used in the FE formulation from Eq. (7). Analogously, in linear structural analysis, the inverse of the density and the inverse of the bulk modulus correspond to the density and Young's modulus, respectively

$$\phi_1 = \gamma_{e,1}^n \times (1-\gamma_{e,2}^n), \quad \phi_2 = \gamma_{e,2}^n \times (1-\gamma_{e,1}^n), \quad 0 \le \gamma_{e,1} \le 1, \quad 0 \le \gamma_{e,2} \le 1 \tag{17}$$

$$\textit{Inverse Density}: \quad \frac{1}{\rho_e(\gamma_{e,1},\gamma_{e,2})} = \frac{1}{\rho_a} + \left(\frac{1}{\rho_s} - \frac{1}{\rho_a}\right)\phi_1 + \left(\frac{1}{\rho_f} - \frac{1}{\rho_a}\right)\phi_2 \tag{18}$$

$$\textit{Inverse Bulk Modulus}: \quad \frac{1}{k_e^{\text{bulk}}(\gamma_{e,1},\gamma_{e,2})} = \frac{1}{k_a^{\text{bulk}}} + \left(\frac{1}{k_s^{\text{bulk}}} - \frac{1}{k_a^{\text{bulk}}}\right)\phi_1 + \left(\frac{1}{k_f^{\text{bulk}}} - \frac{1}{k_a^{\text{bulk}}}\right)\phi_2 \tag{19}$$

where the design variables defined at the eth finite element are denoted by $\gamma_{e,1}$ and $\gamma_{e,2}$. The bulk moduli for solid material and air are denoted by k_s^{bulk} and k_a^{bulk}, respectively and the densities for solid material and air are also denoted by ρ_s and ρ_a, respectively. The interpolated density and bulk modulus are ρ_e and k_e^{bulk}, respectively. The polynomial functions are denoted by ϕ_1 and ϕ_2 for the interpolations of solid material and fibrous material, respectively. As in the conventional SIMP approach, a real number n between 3 and 4 is set for the penalty value. After TO, the design variables converge to zeros and ones, and once stable, these values indicate whether each point of a design domain is air, solid material, or fibrous material. It should be mentioned that the density and the bulk modulus of the solid domain were set to 10^7 and 10^9 times those of air based on the conclusions of the research in Ref. [23]. Those conclusions were also tested for this study, although they are not presented in this paper.

3.2.1. The second SIMP-based interpolation functions: heuristic interpolation functions for fibrous materials

By means of the first SIMP-based interpolation functions from Eqs. (17)–(19), internal solid structures and fibrous structures can appear independently; fibrous materials can freely appear in a design domain as shown in Fig. 4(a). Moreover, since the rigidity and stiffness values of fibrous material are commonly smaller than those of solid material, it is often essential for fibrous material to be attached to a relatively stiffer internal solid structure for practical applications as shown in Fig. 4(b). From a topology optimization point of view, this factor is a difficult and non-differentiable condition to consider and implement because an optimal topology of internal solid structure should be determined by TO, without prior specifications. To achieve this design purpose and objective, this research presents new interpolation functions with a window function, which is defined as the power of the filtered design variables via a simple density filter, as from Eqs. (20)–(23). There are two key points to consider for this new function: first, the filtered and the unfiltered design variables are used simultaneously in Eqs. (22) and (23), and second, an optimization process does not take into account the sensitivity values of the filtered densities by setting them to zero. Although this technique is a heuristic one, it can still be used as an interpolation scheme to confine the appearance of fibrous material to only the boundaries of the internal solid structures. Because the complex density and bulk modulus of the Helmholtz equation are multiplied by the simple density filter, they do no account for the pressure attenuation from fibrous materials appearing outside the boundaries of the solid

Table 1
Interpolated material properties for fibrous material.

	Acoustic domain	Solid domain (rigid wall [23])	Fibrous domain
Density	ρ_a	$\rho_s = \rho_a \times 10^7$	ρ_f
Bulk modulus	k_a^{bulk}	$k_s^{\text{bulk}} = k_a^{\text{bulk}} \times 10^9$	k_f^{bulk}

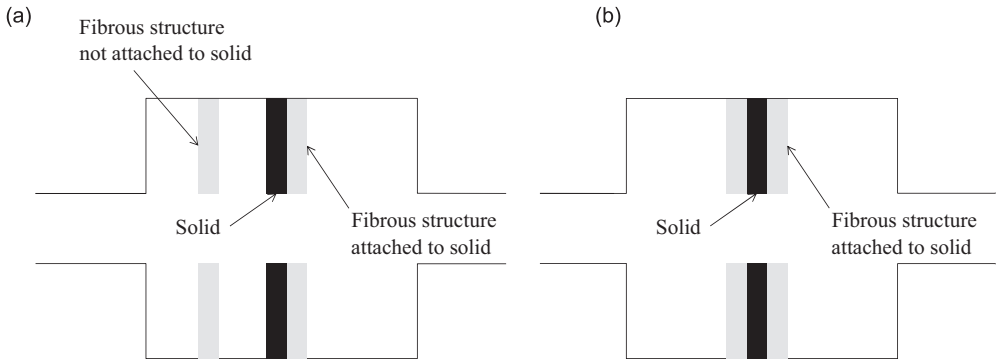

Fig. 4. An example of a fibrous structure attached to an internal solid structure: (a) fibrous structures independent of solid structures and (b) fibrous structures confined at the boundaries of solid structures.

structure. The width of the fibrous material boundaries is controlled by a filter radius, rmin, which is set manually. Although this heuristic approach was developed based on only the above physical observations, it can still be utilized as an engineering design tool. Consequently, postprocessing should be performed on the actual response calculation. Note that in the following method, the penalization n_f in Eq. (21) was fixed to 3 based on the results of several optimization tests

$$\phi_1 = \gamma_{e,1}^n \times (1-\gamma_{e,2}^n), \quad \phi_2 = \gamma_{e,2}^n \times (1-\gamma_{e,1}^n) \tag{20}$$

$$\phi_3 = (\tilde{\boldsymbol{\gamma}})^{n_f} \quad \text{where } n_f \text{ penalization factor}$$

$$\tilde{\boldsymbol{\gamma}} = \Xi(\boldsymbol{\gamma}) = \left\{ \tilde{\gamma}_{e,1} : \tilde{\gamma}_{e,1} = \sum_{\substack{\text{for all } k \text{ satisfying} \\ \text{dist}_{e,k} \le r_{\min}}} \gamma_{k,1}/N_e, \quad e = 1,2,\ldots,NE \right\} \tag{21}$$

where Ξ is the density filter and $\text{dist}_{e,k}$ is the distance between the eth and the kth elements, N_e is the number of elements inside a filter, and and $r_{\min}$ is the filter radius.

$$\textit{Inverse Density}: \quad \frac{1}{\rho_e(\gamma_{e,1},\gamma_{e,2})} = \frac{1}{\rho_a} + \left[\left(\frac{1}{\rho_s} - \frac{1}{\rho_a} \right) \phi_1 + \left(\frac{1}{\rho_f} - \frac{1}{\rho_a} \right) \phi_2 \right] \phi_3 \tag{22}$$

$$\textit{Inverse Bulk Modulus}: \quad \frac{1}{k_e^{\text{bulk}}(\gamma_{e,1},\gamma_{e,2})} = \frac{1}{k_a^{\text{bulk}}} + \left[\left(\frac{1}{k_s^{\text{bulk}}} - \frac{1}{k_a^{\text{bulk}}} \right) \phi_1 + \left(\frac{1}{k_f^{\text{bulk}}} - \frac{1}{k_a^{\text{bulk}}} \right) \phi_2 \right] \phi_3 \tag{23}$$

3.2.2. Sensitivity analysis—transmission loss

To obtain the gradient values of the objective, the adjoint sensitivity analysis is performed. Because the system matrix and the responses are complex, the complex sensitivity analysis should be carried out. In this section, the sensitivity analysis for the transmission loss is presented. The sensitivity analysis for other object functions can be obtained by a similar approach. First of all, let us define the vectors giving the pressures, p_1, p_2 and p_3, at the three points as follows:

$$p_1 = \mathbf{L}_1^{\mathrm{T}}\mathbf{X}, \quad p_2 = \mathbf{L}_2^{\mathrm{T}}\mathbf{X}, \quad p_3 = \mathbf{L}_3^{\mathrm{T}}\mathbf{X} \tag{24}$$

By neglecting the effect of the input and output the areas (the equal areas), the transmission loss can be represented as follows:

$$\mathbf{AX} = \frac{1}{\mathrm{e}^{\mathrm{i}kx_{12}}\left(1-\mathrm{e}^{-2\mathrm{i}kx_{12}}\right)}(\mathbf{L}_1 - \mathbf{L}_2 \times \mathrm{e}^{-\mathrm{i}kx_{12}}) \tag{25}$$

$$\mathrm{TL} = 20\log\left(\left|\frac{p_i}{p_3}\right|\right) = 10[\log(\mathrm{conj}(\mathbf{AX}^{\mathrm{T}}\cdot\mathbf{X}) \times (\mathbf{AX}^{\mathrm{T}}\cdot\mathbf{X})) - \log(\mathrm{conj}(p_3) \times p_3)] \tag{26}$$

where the auxiliary vector is **AX** and the conjugate operator is "conj". For the adjoint variables, we calculate the following two adjoint variables:

$$[\mathbf{K}(\omega) - \omega^2\mathbf{M}(\omega)]\boldsymbol{\lambda}_1 = -\frac{10\mathrm{conj}(\mathbf{AX}^{\mathrm{T}})\cdot\mathrm{conj}(\mathbf{X})}{\mathrm{conj}(\mathbf{AX}^{\mathrm{T}})\cdot\mathrm{conj}(\mathbf{X}^{\mathrm{T}})\cdot\mathbf{AX}^{\mathrm{T}}\cdot\mathbf{X}}\mathbf{AX} + \frac{10\cdot\mathrm{conj}(p_3)}{\mathrm{conj}(p_3)\cdot p_3}\mathbf{L}_3 \tag{27}$$

$$\mathrm{conj}([\mathbf{K}(\omega) - \omega^2\mathbf{M}(\omega)])\boldsymbol{\lambda}_2 = \mathrm{conj}\left(-\frac{10\mathrm{conj}(\mathbf{AX}^{\mathrm{T}})\cdot\mathrm{conj}(\mathbf{X})}{\mathrm{conj}(\mathbf{AX}^{\mathrm{T}})\cdot\mathrm{conj}(\mathbf{X})\cdot\mathbf{AX}^{\mathrm{T}}\cdot\mathbf{X}}\mathbf{AX} + \frac{10\cdot\mathrm{conj}(p_3)}{\mathrm{conj}(p_3)\cdot p_3}\mathbf{L}_3 \right) \tag{28}$$

Then the sensitivity variable of the transmission with respect to the design variable γ can be computed as follows:

$$\frac{\partial \mathrm{TL}}{\partial \gamma} = \mathrm{real}\left(\boldsymbol{\lambda}_1^{\mathrm{T}}\left(\frac{\partial \mathbf{K}}{\partial \gamma} - \omega^2 \frac{\partial \mathbf{M}}{\partial \gamma}\right)\mathbf{X} + \boldsymbol{\lambda}_2^{\mathrm{T}}\left(\mathrm{conj}\left(\frac{\partial \mathbf{K}}{\partial \gamma}\right) - \omega^2 \mathrm{conj}\left(\frac{\partial \mathbf{M}}{\partial \gamma}\right)\right)\mathrm{conj}(\mathbf{X})\right) \tag{29}$$

4. Acoustic topology optimization examples

To test the validity of the present approach in ATO, several acoustic optimization problems were solved and are presented here. For the gradient-based optimizer, the Method of Moving Asymptotes (MMA) was used [34]. The design domain, geometry, and material properties in these examples were chosen for their relevance to real engineering applications so as to show the importance of using fibrous material in ATO. Unless otherwise stated, the initial design variables satisfying the mass constraints are employed.

4.1. Example 1: Acoustic example (muffler)

For the first numerical example, the improvement of the pressure attenuation of a two-dimensional muffler in Fig. 5 was considered by designing optimal solid and fibrous structures inside its internal expansion chamber. Compared to designs using only solid materials, it was expected that the pressure attenuation of this predominantly reactive muffler could be enhanced with the inclusion of fibrous material in the gray-shaded design domain in Fig. 5. As an objective function, the transmission loss (TL) was calculated by the "3-point method." For the sensitivity calculation, the adjoint variable method was employed.

Fig. 6 shows the two optimized layouts with either solid or porous materials ($\sigma=1000$ Rayleighs/m) at $\omega=1000$ rad/s. When fibrous materials were not considered, a similar design to the one presented in Ref. [23] was obtained, while a different topology, as seen in Fig. 6(b), was obtained when fibrous materials were included. The investigation of the transmission curves of each design in Fig. 6(c) shows that the higher transmission loss can be achieved using both the solid and the porous materials. Because of the damping effects of the porous material, the usage of the porous material does not change the transmission curve much. With the solid wall, however, the significant changes are observed. In this example, the penalization of the SIMP method is enough to obtain the designs with few intermediate design variables. For the purpose of illustration, the solid structure and the fibrous structure have been rendered as black and gray, respectively.

Fig. 7 shows several layouts optimized at three angular speeds of the incoming wave with fibrous materials as well as solid materials. Also the mesh size effect is test in Fig. 8. It seems that a sufficient refined mesh provides the similar results. Compared with the TL curve of the design using only solid materials (Figs. 6(a), 9(d), and 10), a higher pressure attenuation was achievable by adding fibrous materials. Furthermore, at $\omega=1000$ rad/s, the fibrous material remained attached to the solid structures, whereas the fibrous material appeared to pull apart from the solid internal structures at $\omega=2000$ rad/s and $\omega=3000$ rad/s. Fig. 9(d) shows the transmission loss curves of these designs. Each design was optimized for its excitation angular velocity, and consequently, a higher pressure attenuation was obtained.

As stated in the previous section, to maintain the structural rigidity of a design, it is sometimes necessary to attach fibrous material to a solid structure. To achieve this design objective, the second interpolation functions of Eqs. (22) and (23) were applied using a filter radius that was 16 times larger than the initial finite element size, as illustrated in Fig. 9. As shown, the smooth fibrous materials were positioned at the boundaries of the solid structures. Because the complex density and bulk modulus of the Helmholtz equation were multiplied by the simple density filter, the pressure attenuation from the fibrous materials appearing outside the boundaries of the solid structure was not accounted for. As a consequence, the fibrous material did not separate from the solid. It is worthwhile to note that the spatial locations of the four solid bars in the upper and lower design domains of Figs. 7(b) and 9(b) for $\omega=2000$ rad/s are similar to each other. On the contrary, rather than the six bars in Fig. 7(b), four bars consisting of solid and fibrous materials were obtained in Fig. 9(c) at $\omega=3000$ rad/s, which has many similarities to Fig. 9(b) at $\omega=2000$ rad/s, by the present optimization framework. This result was first thought to be the consequence of bad local optima due to the introduced heuristic filter; however, an investigation of the TL curves of the design revealed that because the pressure attenuation of the design for $\omega=3000$ rad/s was high enough, the optimizer removed the center bars for this design and changed the positions of the two bars.

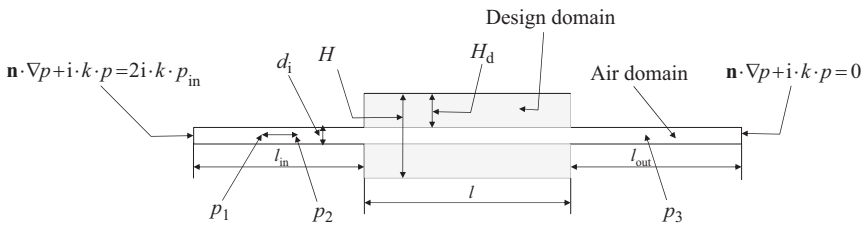

Fig. 5. The muffler optimization example. A muffler geometry ($\rho_a=1.25$ kg/m^3, $c_a=343$ m/s, $\sigma=1000$ Rayleighs/m, $l=1.2$ m, $l_{\mathrm{in}}=l_{\mathrm{out}}=1.0$ m, $H_d=0.2$ m, $H=0.5$ m, $d_i=0.1$ m, $x_{12}=0.1$ m).

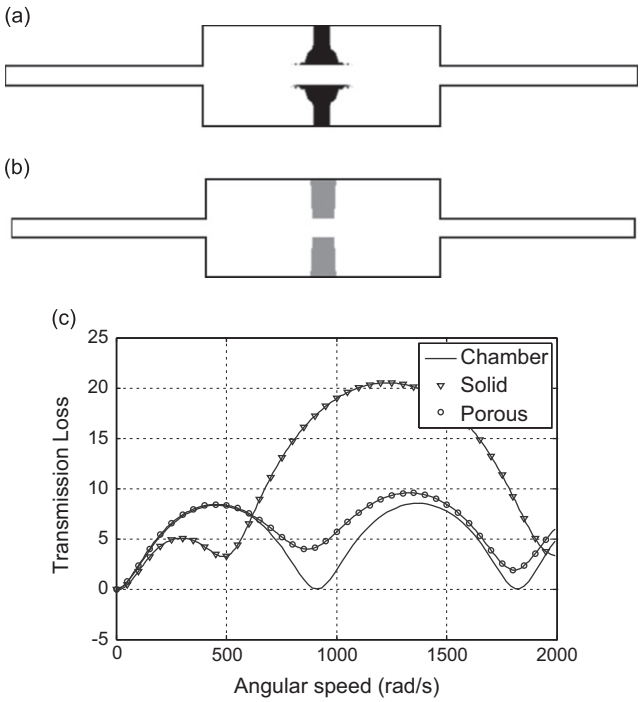

Fig. 6. The optimized layouts at $\omega=1000$ rad/s with only (a) solid material ($\beta_{\text{solid}}=0.1$, $\beta_{\text{fibrous}}=0.0$), (b) fibrous material ($\beta_{\text{solid}}=0.0$, $\beta_{\text{fibrous}}=0.1$, $\sigma=1000$ Rayleighs/m) and (c) the transmission curves.

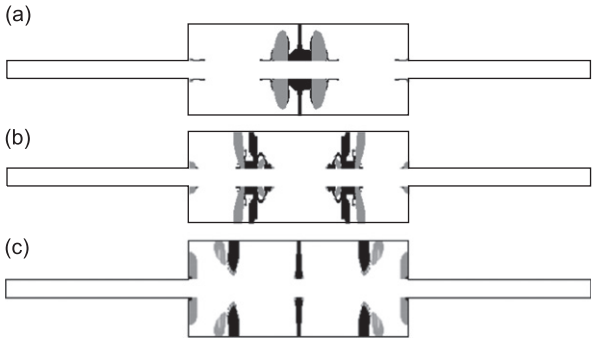

Fig. 7. Acoustic topology optimization results ($\rho_a=1.25$ kg/m^3, $c_a=343$ m/s, $\sigma=1000$ Rayleighs/m, $\beta_{\text{solid}}=0.1$, $\beta_{\text{fibrous}}=0.1$, the initial design variables: 0.1 satisfying the mass constraints) at (a) $\omega=1000$ rad/s, (b) $\omega=2000$ rad/s and (c) $\omega=3000$ rad/s.

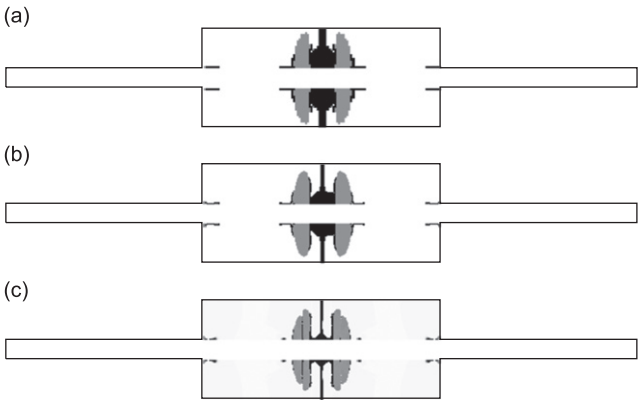

Fig. 8. The mesh dependency. (a) The result with 0.01 m $\times$ 0.01 m elements, (b) the result with 0.005 m $\times$ 0.005 m and (c) the result with 0.0025 m $\times$ 0.0025 m.

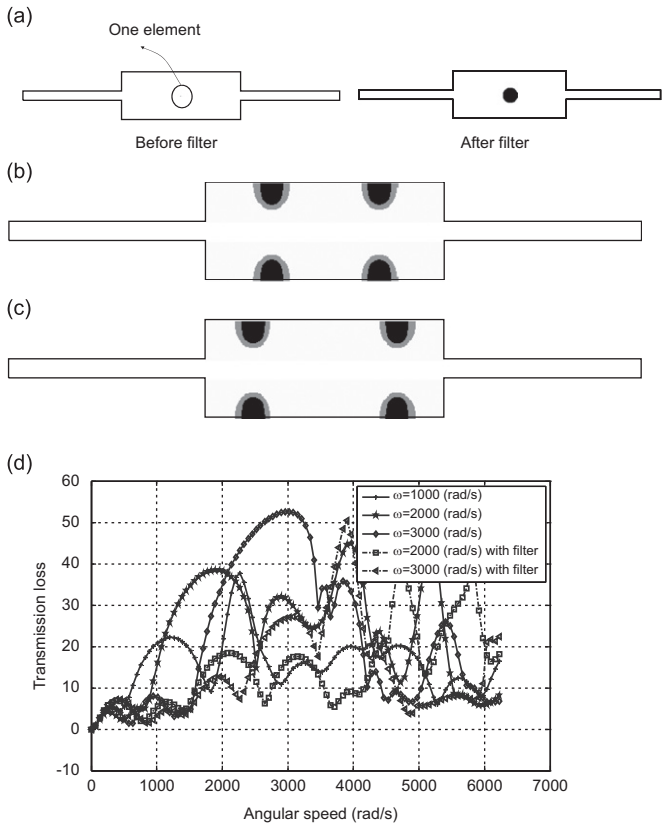

Fig. 9. Optimized designs with the heuristic filter and the transmission loss curves of the designs. (a) An example of the filter (filter radius = 16 times the element size), (b) an optimized design with the filter ($\omega = 2000$ rad/s), (c) an optimized design with the filter ($\omega = 3000$ rad/s), and (d) the TL responses of the obtained designs.

Fig. 10 tests the effect of the flow resistivity values on the optimized layouts for $\omega = 1000$ rad/s. As illustrated, the different layouts can be obtained. By increasing the magnitude of flow resistivity value, the higher transmission losses are obtainable (higher damping effect). Furthermore, it seems that the porous materials are aligned in the y-direction by increasing the magnitude of flow resistivity value.

Only topology optimization for a single excitation frequency being considered until now, it is also possible to extend the above optimization formulation for a finite interval of excitation frequency. To show the possibility, the following optimization problem is considered by setting the integration of the transmission loss and the variation over a finite frequency interval as the objective function as follows:

$$\begin{aligned}
&\text{Min } \phi(\mathbf{X}) = \alpha \cdot \text{Mean} + \beta \cdot \text{Variance} \\
&\text{Subject to } \sum_{e=1}^{NE} \gamma_{e,1} v_e \Big/ \sum_{e=1}^{NE} v_e - \beta_{\text{solid}} \le 0 \\
&\sum_{e=1}^{NE} \gamma_{e,2} v_e \Big/ \sum_{e=1}^{NE} v_e - \beta_{\text{fibrous}} \le 0 \\
&\text{Mean} = \frac{\int_{\omega_s}^{\omega_e} \text{TL}(\omega)\,\mathrm{d}\omega}{\omega_e - \omega_s} \\
&\text{Variance} = \frac{\int_{\omega_s}^{\omega_e} (\text{TL}(\omega))^2\,\mathrm{d}\omega}{\omega_e - \omega_s} - \left(\frac{\int_{\omega_s}^{\omega_e} \text{TL}(\omega)\,\mathrm{d}\omega}{\omega_e - \omega_s} \right)^2
\end{aligned} \tag{30}$$

where the starting frequency and the end frequency are denoted by ω_s and ω_e, respectively and the integrations of the above functions are done in the equal abscissa. The number of the integration points (ω_k) is NP. Both the mean transmission loss and the variation of the transmission loss over the frequency interval are considered in the above optimization formulation. With the mean transmission loss only, a design with a higher peak is obtained. To obtain a design with similar transmission loss for the frequency interval, the objective function is modified by inserting the variation. With this modification, it is possible to obtain the design with the lower but equal transmission losses for the frequency domain of interest. The scaling parameters of the two objectives are α and β; the parameters are chosen after

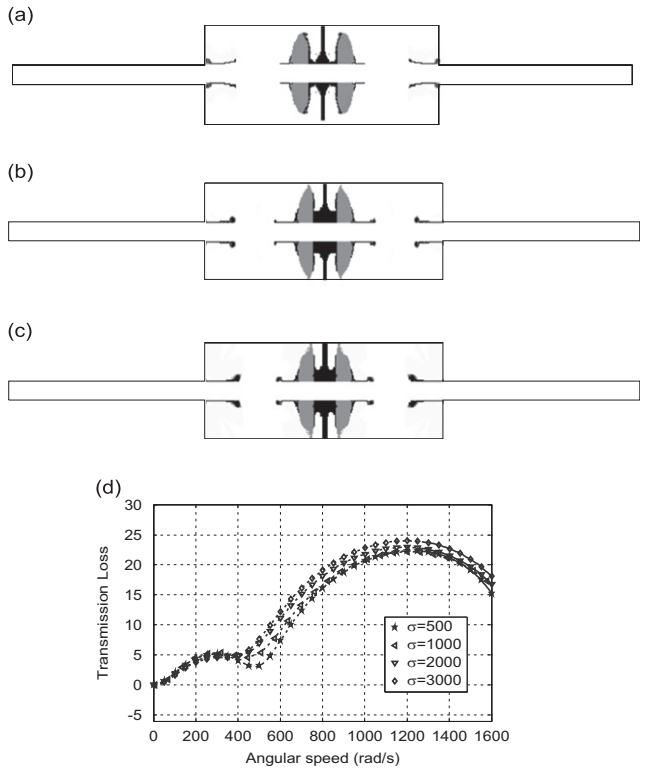

Fig. 10. Optimized layouts with several different flow resistivity values for $\omega=1000$ rad/s and $\beta_{solid}=0.1$, $\beta_{fibrous}=0.1$. (a) The flow resistivity values of $\sigma=500$ Rayleighs/m, (b) the flow resistivity values of $\sigma=2000$ Rayleighs/m, (c) the flow resistivity values of $\sigma=3000$ Rayleighs/m and (d) the frequency response curves of the designs.

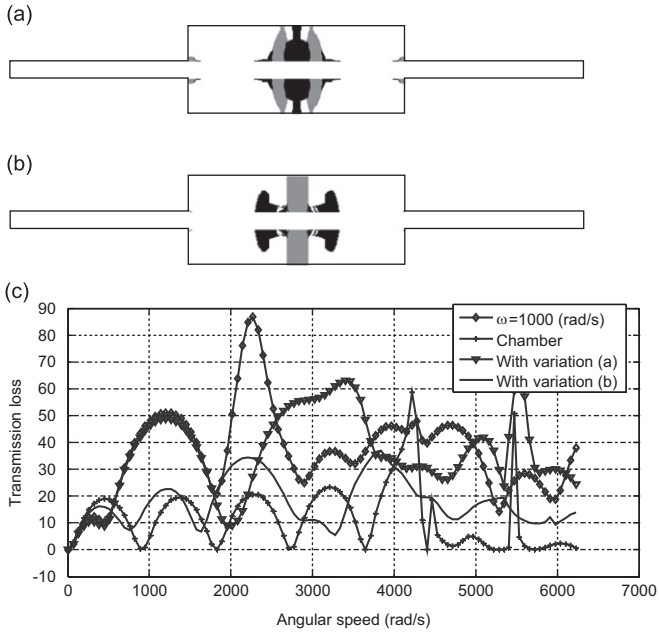

Fig. 11. A numerical example for a finite interval of excitation frequency ($\omega_s=700$ rad/s, $\omega_e=1300$ rad/s, frequency sampling : 100 rad/s). (a) An obtained layout with $\alpha=-1$ and $\beta=+1$, (b) an obtained layout with $\alpha=-1$ and $\beta=+10$) and (c) the frequency response curves.

several heuristic numerical tests. To test the application of the above formulation, the angular velocity interval from 700 rad/s to 1300 rad/s is tested in Fig. 11. One of the reasons of the choice of this frequency interval is due to that the design in Fig. 7(a) has a high peak in 1000 rad/s and we want to show that the above optimization formulation can present

a new design considering the variance of the TL as well as the mean of the TL. The obtained design and the frequency responses of the design are shown in Fig. 11(a), (b) and (c), respectively.

4.2. Example 2: Wall design minimizing the pressure integral of a specified zone

For the second numerical example, the present ATO framework was employed to find optimal solid and fibrous material distributions inside a middle rectangular wall that minimized the pressure integral inside a small circle, found on the right-hand side of Fig. 12(a). The assumed sound source is represented by the circle on the left in Fig. 12(a). For reference, the optimal material distributions with either solid material or fibrous material are found in Fig. 12(b). Fig. 12(c) shows the optimal topology design together with the fibrous and solid materials. In the specific example shown in Fig. 12(c), the solid material distribution was not affected by the fibrous material distribution. Furthermore the frequency responses of solid

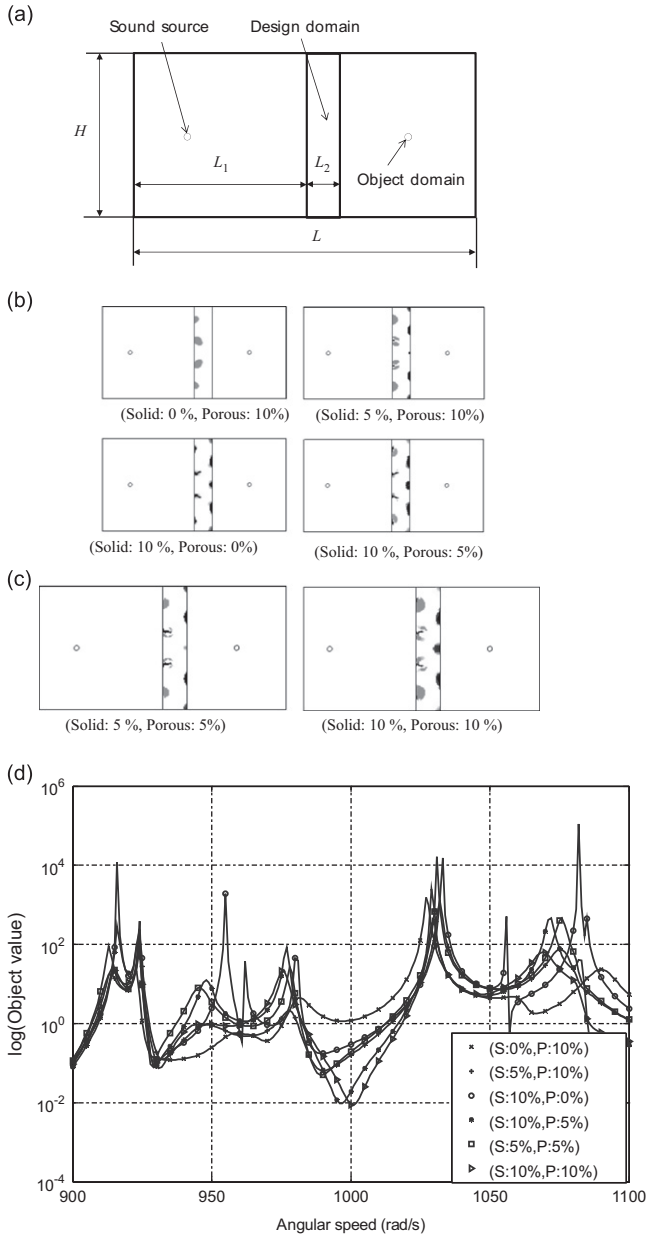

Fig. 12. Optimization problem of wall structure minimizing the pressure integral of a specified zone. (a) The problem definition (ρ_a=1.25 kg/m^3, c_a=343 m/s, σ=1000 Rayleighs/m, L=10 m, L_1=5.0 m, L_2=1.0 m, H=5.0 m, σ=1000 Rayleighs/m, ω=1000 rad/s), (b) reference designs with only solid or fibrous material, (c) optimal layouts with the two materials (β_{solid}=0.05, β_{fibrous}=0.05), and (d) the responses of the designs.

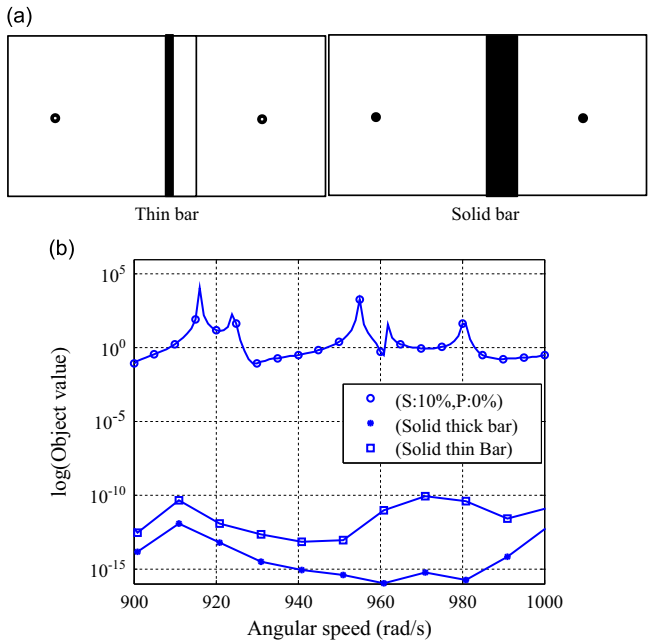

Fig. 13. A local optima issue of the present acoustic topology optimization: (a) a thin solid box and solid bar and (b) the frequency response curves.

bar filled inside the design domain and straight thin bar of 0.1 m are compared in Fig. 13.[3] As shown, the objective values of the solid bar and the straight thin bar are much lower than those of the present designs. This clearly shows that the designs are local optima and the investigation of the intermediate designs reveals that the present ATO or the similar topology optimization methods distributes solid and fibrous materials to move areas with zero or near zero pressure values to the design domain.

Furthermore, to confine the fibrous material to the boundaries of the solid internal structures, the second interpolation functions were multiplied by the filtered density window are shown in Fig. 14. As expected and observed in the first numerical example, the design with these second interpolation functions had a lower object function than that of the design with the first interpolation functions but the fibrous material only appeared at the boundaries of the solid structure in the second case. Fig. 14(c) shows the pressure integrals of each design with respect to the excitation frequencies. As expected, with the heuristic filter, the performances are degraded. In the examples, the effects of the mass ratios of the solid and the porous materials are investigated by varying their ratios. Comparing the performances of the, it turns out that the solid has much more influence than the porous.

5. Conclusions

Because acoustical fibrous materials contribute greatly to the noise characteristics of a whole acoustic system, designing an optimal acoustic system that considers the pressure attenuation from porous or fibrous materials is an important engineering task. Despite abundant research on acoustic topology optimization (ATO), it is rare to employ an empirical formulation for ATO. Thus, the focus of the present study was to utilize the empirical Delany–Bazley formulation for ATO.

Some analytical and empirical material models depend on physical interpretations of the fibrous materials of interest. In this research, it is assumed that the elastic frame that forms the structure for a fibrous material can be considered a rigid frame whose material properties are well described by the empirical Delany–Bazley material model. By interpolating the density and the bulk modulus values with respect to the TO design variables, optimal topologies of both the fibrous and solid structures were obtained. For topology optimization, the SIMP-based interpolation functions with multiple materials were used without loss of generality. Furthermore, by confining fibrous materials to only the perimeters or rims of the solid structure, new heuristic interpolation functions were presented. Then, by applying these heuristic interpolation functions, it was possible to design both a solid structure and a porous structure attached to the solid structure. In

[3] Proposed by an anonymous reviewer.

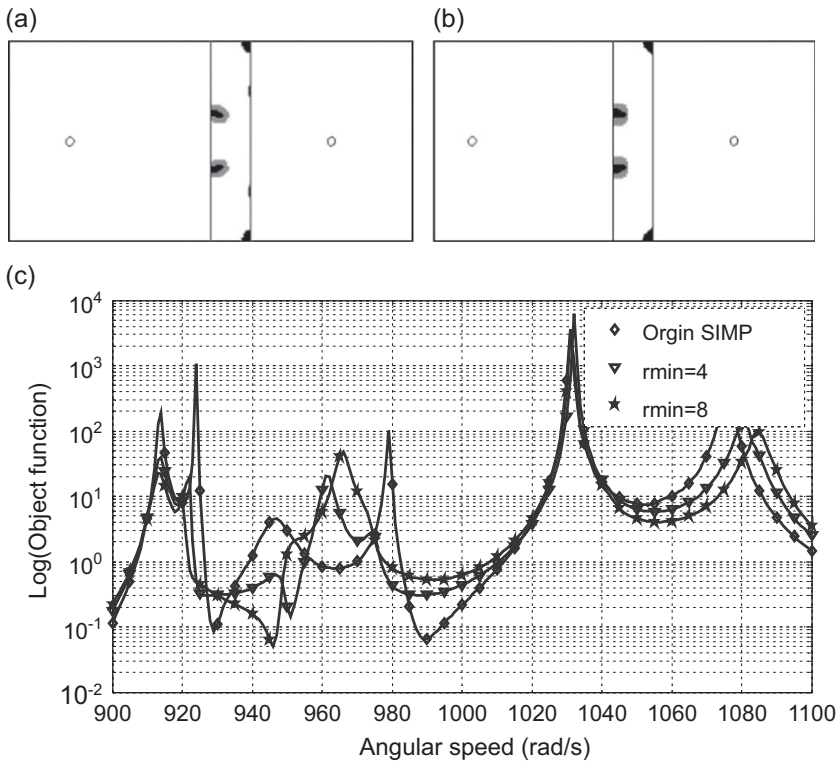

Fig. 14. Optimized designs with the heuristic filter and the object curves of the optimized designs ($\beta_{\text{solid}}=0.05$, $\beta_{\text{fibrous}}=0.05$). (a,b) The optimized designs with the filter ($r_{\min}=4\times$ element size and $r_{\min}=8\times$ element size) ($\omega=1000$ rad/s) and (c) the responses of each design.

conclusion, we have presented an acoustic topology optimization method that considers the pressure attenuation through a fibrous material and can be simulated by the empirical Delany–Bazley material model.

Acknowledgements

This work was supported by the National Research Foundation of Korea(NRF) grant funded by the Ministry of Education, Science and Technology (No. 2012R1A1A2A10038803).

References

[1] M.P. Bendsøe, O. Sigmund, *Topology, Optimization: Theory, Methods, and Applications*, Springer, Berlin, New York, 2003.
[2] T. Borrvall, J. Petersson, Topology optimization of fluids in Stokes flow, *International Journal for Numerical Methods in Fluids* 41 (2003) 77–107.
[3] E. Lund, H. Moller, L.A. Jakobsen, Shape design optimization of stationary fluid–structure interaction problems with large displacements and turbulence, *Structural and Multidisciplinary Optimization* 25 (2003) 383–392.
[4] G.H. Yoon, J.S. Jensen, O. Sigmund, Topology optimization of acoustic–structure interaction problems using a mixed finite element formulation, *International Journal for Numerical Methods in Engineering* 70 (2007) 1049–1075.
[5] A. Gerstenberger, W.A. Wall, An eXtended Finite Element Method/Lagrange multiplier based approach for fluid–structure interaction, *Computer Methods in Applied Mechanics and Engineering* 197 (2008) 1699–1714.
[6] G.H. Yoon, O. Sigmund, A monolithic approach for topology optimization of electrostatically actuated devices, *Computer Methods in Applied Mechanics and Engineering* 197 (2008) 4062–4075.
[7] G.H. Yoon, Topology optimization for stationary fluid–structure interaction problems using a new monolithic formulation, *International Journal for Numerical Methods in Engineering* 82 (2010) 591–616.
[8] J.K. Guest, J.H. Prevost, Topology optimization of creeping fluid flows using a Darcy–Stokes finite element, *International Journal for Numerical Methods in Engineering* 66 (2006) 461–484.
[9] S. Wang, K. Koo, B. Pluymers, W. Desmet, Vibro-acoustic design sensitivity analysis using the wave-based method, *Journal of Sound and Vibration* 330 (2011) 4340–4351.
[10] M.L. Munjal, *Acoustics of Ducts and Mufflers with Application to Exhaust and Ventilation System Design*, Wiley, New York, 1987.
[11] L.E. Kinsler, *Fundamentals of Acoustics*, 3rd edition, Wiley, New York, 1982.
[12] Y.J. Kang, J.S. Bolton, Finite-element modeling of isotropic elastic porous materials coupled with acoustical finite-elements, *Journal of the Acoustical Society of America* 98 (1995) 635–643.
[13] J.F. Allard, N. Atalla, *Propagation of Sound in Porous Media: Modelling Sound Absorbing Materials*, 2nd edition, Wiley, Hoboken, NJ, 2009.
[14] B. Zhang, T.N. Chen, Calculation of sound absorption characteristics of porous sintered fiber metal, *Applied Acoustics* 70 (2009) 337–346.
[15] Y. Miki, Acoustic properties of porous materials—generalizations of empirical models, *Acoustical Society of Japan* 11 (1990) 25–28.

[16] J.F. Allard, Y. Champoux, New empirical equations for sound-propagation in rigid frame fibrous materials, *Journal of the Acoustical Society of America* 91 (1992) 3346–3353.
[17] F. Alton, *The Master Handbook of Acoustics*, 4th edition, McGraw-Hill, New York, 2001.
[18] E. Wadbro, M. Berggren, Topology optimization of an acoustic horn, *Computer Methods in Applied Mechanics and Engineering* 196 (2006) 420–436.
[19] Y.Y. Kim, J.S. Lee, E. Kim, J.S. Kim, Y.J. Kang, Optimal poroelastic layer sequencing for sound transmission loss maximization by topology optimization method, *Journal of the Acoustical Society of America* 122 (2007) 2097–2106.
[20] Y.Y. Kim, J.S. Lee, J.S. Kim, Y.J. Kang, Two-dimensional poroelastic acoustical foam shape design for absorption coefficient maximization by topology optimization method, *Journal of the Acoustical Society of America* 123 (2008) 2094–2106.
[21] T. Yamamoto, S. Maruyama, S. Nishiwaki, M. Yoshimura, Topology design of multi-material soundproof structures including poroelastic media to minimize sound pressure levels, *Computer Methods in Applied Mechanics and Engineering* 198 (2009) 1439–1455.
[22] O. Sigmund, J.S. Jensen, Design of acoustic devices by topology optimization, *Proceedings of Fifth World Congress on Structural and Multidisciplinary Optimization (WCSMO 5)*, 2003, pp. 267–268.
[23] J.W. Lee, Y.Y. Kim, Topology optimization of muffler internal partitions for improving acoustical attenuation performance, *International Journal for Numerical Methods in Engineering* 80 (2009) 455–477.
[24] M.B. Duhring, J.S. Jensen, O. Sigmund, Acoustic design by topology optimization, *Journal of Sound and Vibration* 317 (2008) 557–575.
[25] M.A. Biot, Theory of propagation of elastic waves in a fluid–saturated porous solid, *Journal of the Acoustical Society of America* 28 (1955) 168–191.
[26] N. Olhoff, J.B. Du, Minimization of sound radiation from vibrating bi-material structures using topology optimization, *Structural and Multidisciplinary Optimization* 33 (2007) 305–321.
[27] A. Baz, W. Akl, A. El-Sabbagh, K. Al-Mitani, Topology optimization of a plate coupled with acoustic cavity, *International Journal of Solids and Structures* 46 (2009) 2060–2074.
[28] M.H. Fouladi, M. Ayub, M.J.M. Nor, Analysis of coir fiber acoustical characteristics, *Applied Acoustics* 72 (2011) 35–42.
[29] J. Alba, J. Ramis, M.T. Lorenzana, R. del Rey, Proposal a empirical model for absorbent acoustical materials, *Revista Internacional de Métodos Numéricos para Cálculo y Diseño en Ingeniería* 24 (2008) 147–162.
[30] C.W. Lim, C. Cheong, S.R. Shin, S. Lee, Time-domain numerical computation of noise reduction by diffraction and finite impedance of barriers, *Journal of Sound and Vibration* 268 (2003) 385–401.
[31] M.E. Delany, E.N. Bazley, Acoustical properties of fibrous absorbent materials, *Applied Acoustics* 3 (1970) 105–116.
[32] K.O. Ballagh, Acoustical properties of wool, *Applied Acoustics* 48 (1996) 101–120.
[33] C.N. Wang, Numerical decoupling analysis of a resonator with absorbent material, *Applied Acoustics* 58 (1999) 109–122.
[34] K. Svanberg, The method of moving asymptotes—a new method for structural optimization, *International Journal for Numerical Methods in Engineering* 24 (1987) 359–373.